Journal of Applied Physics

RESEARCH ARTICLE | SEPTEMBER 04 2020

Mo/Ti multilayer Bragg reflector for $LiNbO_3$ film bulk acoustic wave resonators

Xiaoyuan Bai ; Yao Shuai ; Lu Lv; Shitian Huang; Ying Xing; Jiaoling Zhao; Wenbo Luo ; Chuangui Wu ; Tao Yang; Wanli Zhang

J. Appl. Phys. 128, 094503 (2020)
https://doi.org/10.1063/5.0011954

Journal of Applied Physics ARTICLE scitation.org/journal/jap

Mo/Ti multilayer Bragg reflector for $LiNbO_3$ film bulk acoustic wave resonators

Cite as: J. Appl. Phys. **128**, 094503 (2020); doi: 10.1063/5.0011954
Submitted: 26 April 2020 · Accepted: 22 August 2020 ·
Published Online: 4 September 2020

Xiaoyuan Bai,[1] Yao Shuai,[1,a)] Lu Lv,[1] Shitian Huang,[1] Ying Xing,[1] Jiaoling Zhao,[2] Wenbo Luo,[1] Chuangui Wu,[1,a)] Tao Yang,[3] and Wanli Zhang[1]

AFFILIATIONS

[1]State Key Laboratory of Electronic Thin Films and Integrated Devices, University of Electronic Science and Technology of China, Chengdu 611731, China
[2]Shanghai Institute of Optics and Fine Mechanics, Chinese Academy of Sciences, Shanghai 201800, China
[3]School of Electronic Science and Engineering, University of Electronic Science and Technology of China, Chengdu 611731, China

[a)]**Authors to whom correspondence should be addressed:** yshuai@uestc.edu.cn and cgwu@uestc.edu.cn

ABSTRACT

A 43° rotated Y-cut $LiNbO_3$ (LN) single-crystal thin film coated with a bottom electrode and a Mo/Ti Bragg reflector is successfully transferred onto the 4-in. LN wafer substrate by means of crystal-ion-slicing (CIS) technique and benzocyclobutene bonding method. The multilayer film is crack-free, and the Mo/Ti reflector shows good acoustic reflection efficiency. A thin film bulk acoustic wave resonator based on the Mo/Ti Bragg reflector and the LN thin film (LN-BAW) is prepared, and the properties are further analyzed. The results indicate that the LN-BAW provides a large K_t^2 of ∼16.63% and the Q-factor and figure-of-merit of the LN-BAW reach 183 and 30.4, respectively.

I. INTRODUCTION

A thin film bulk acoustic wave (BAW) filter,[1] which has attractive advantages such as compact size, low insertion loss, and high out-of-band rejection, has been widely used in the RF front-end modular for mobile communications. A BAW filter consists of a few BAW resonators, and each single resonator has a parallel capacitor-like structure, where a thin piezoelectric thin film is sandwiched by two metals. The resonator converts the electric energy into acoustic energy through the piezoelectric effect, and in this process, the acoustic energy should be well confined within the resonator, thus a high Q value is obtained.

To prevent the dissipation of acoustic energy, the metal-piezoelectric-metal resonator needs to be fabricated on a well-designed acoustic insulation structure. Currently, the Bragg reflector, fabricated by alternative deposition of low acoustic impedance (LAI) and high acoustic impedance (HAI) thin films, is one of the most popular structures. Each HAI or LAI layer has a thickness of quarter wavelength (λ) of the acoustic wave, and acoustic reflection takes place at the interfaces between LAI and HAI, resulting in a low loss of acoustic energy. The reflection coefficient is dependent on the acoustic impedance ratio between the HAI and LAI materials, and the often used structures include W/SiO_2, Mo/SiO_2, Mo/AlN, W/Al, Mo/Al, Mo/Ti, and so on. The all-metal structures are attractive, because the two types of metal can be easily deposited by sputtering within one vacuum chamber; moreover, the conductive Bragg reflector can also act as the bottom electrode of the BAW resonator. Among those all-metal reflectors, Mo/Ti has a relatively small difference of coefficient of thermal expansion (CTE) between the two metals as compared to W/Al or Mo/Al; thus, a low stress is expected after the subsequent high temperature fabrication process of the piezoelectric thin film.

Another factor influencing the performance of the resonator is the piezoelectric layer. So far, most researches focus on the AlN material due to several reasons such as low acoustic loss, high acoustic velocity, and easy deposition with low stress. However, AlN suffers from a low electromechanical coefficient (K_t^2) of ∼6.5%,[2] which limits the bandwidth of the BAW filter. Although the Sc doping raises the K_t^2 up to 12–15%, the dielectric loss is significantly increased.[3] As compared to AlN, $LiNbO_3$ (LN) has a much larger K_t^2, which is promising for wideband applications. LN is strongly anisotropic, thus only some specific orientations possess high K_t^2; for example, Baron reported that the Y-cut LN thin film with a tilting angle of 30°–45° has a K_t^2 of 20–31%.[4] To obtain such a special cut, the layer transfer technique[5,6] has been developed. With this technique, we have previously reported a successful fabrication of Y128- and Y36-cut LN thin film with a thickness below 1 μm.[7] The arising question is the LN film is directly transferred onto a substrate, which is not combined with the bottom electrode and the acoustic reflector; thus, it cannot be used to fabricate a BAW device. Although some research groups reported the LN-based BAW devices, the LN layer is too thick; thus, the resonance frequency is limited below 1 GHz,[8] which is not attractive for wireless communications.

In the present work, the Mo/Ti Bragg reflector and the 43° rotated Y-cut LN thin film are simultaneously transferred onto a substrate, and a LN-BAW resonator is fabricated. The design of the Mo/Ti Bragg reflector is discussed, and the Mo/Ti multilayer is characterized by an atomic force microscope (AFM) and a scanning electron microscope (SEM). Owing to the Mo/Ti Bragg reflector, the LN thin film exhibits a large K_t^2 of 16.63%, and the Q-factor and figure-of-merit (FOM) of the BAW device reach 183 and 30.4, respectively.

II. EXPERIMENTAL

He^+ ions are implanted into a 4-in. 43° rotated Y-cut LN single crystal wafer and the implantation energy is 285 keV, which forms a defective layer with a depth of 900 nm underneath the surface of the LN wafer. On the implanted side of the wafer, Al bottom electrodes and Mo/Ti multilayers are deposited by sputtering. Then, the implanted wafer with Al and Mo/Ti is bonded onto another 4-in. 43° rotated Y-cut LN wafer using benzocyclobutene (BCB) as the adhesive medium. The bonded wafers are annealed at 350 °C in vacuum for 3 h, during the annealing, the implanted LN wafer splits along the defective layer induced by the He^+ implantation; as a result, a 900 nm-thick 43° rotated Y-cut LN thin film with the Al bottom electrode and the Mo/Ti multilayer is transferred onto a LN substrate. On the surface of the LN thin film, the Al top electrode is sputtered and patterned, and finally LN-BAW devices with the Mo/Ti Bragg reflector are obtained. The above process is illustrated in Fig. 1.

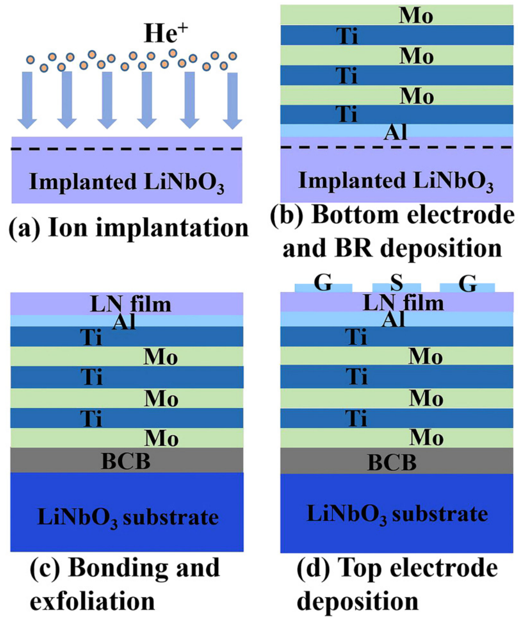

FIG. 1. The processing of the BAW resonator. (a) Ion implantation, (b) bottom electrode and Bragg reflector (BR) deposition, (c) bonding and exfoliation, and (d) top electrode deposition.

III. RESULTS AND DISCUSSION

The quality of the Mo/Ti multilayer significantly influences the performance of the resonator, including the surface roughness and the thickness accuracy. The surface morphology of the Mo/Ti layers is characterized by AFM. In order to analyze the deposition quality of Mo/Ti, two types of experimental regions are fabricated and measured as shown in Figs. 2(a) and 2(c), one is the region above the bare implanted LN, and the other one is above the patterned Al bottom electrode. In both regions, homogenous grains are observed on the surface of the top Mo layer, and the grain size of the latter region is obviously larger than the former [Figs. 2(b) and 2(d)]. However, the surface roughness (RMS) of the latter region (5.47 nm) is slightly smaller than the former (6.75 nm), which is likely due to a better lattice match between the metal Al and Mo/Ti.

With the patterned Al bottom electrode and the Mo/Ti multilayers, a 900 nm-thick LN thin film is successfully transferred onto another LN wafer as shown in Fig. 3(a). It can be seen that LN thin film with the metallic multilayers is crack-free, which is qualified for the fabrication of BAW resonator. The cross-sectional image of the wafer is shown in Fig. 3(b). The thicknesses of the Ti and Mo layers are designed to be 0.46 μm and 0.47 μm, according to the $\lambda/4$ law, in which the acoustic wavelength λ is defined as v/f. The efficiency of acoustic reflection by the Mo/Ti Bragg reflector is verified by a finite element method (FEM) simulation, and the simulation result is illustrated by the blue curve in Fig. 3(c). The distribution of the standing wave amplitudes along with the out-of-plane direction is indicated by the y axis. It can be seen that the standing wave is significantly suppressed within the first Mo/Ti cycle, and the standing wave amplitude is nearly zero after the whole three cycles, revealing the leak of the acoustic energy to substrate can be ignored; thus, the Mo/Ti Bragg reflector is efficient for the acoustic reflection. However, the thicknesses of the Mo/Ti layers inevitably have deviations [Fig. 3(b)] from the designed values due to the fabrication processing, and it may influence the reflection efficiency of the acoustic energy. The practical thickness obtained by the cross-sectional image is adopted in the FEM model replacing the designed thickness, and the corresponding distribution of standing wave amplitude is illustrated by the red curve in Fig. 3(c). It can be seen that the standing wave amplitude in the Bragg reflector layers with practical thickness is slightly larger than the type with designed thickness. Nevertheless, the amplitude still reaches zero after three cycles, which suggests that there is barely leak of acoustic energy into substrates. It has been reported that the deviation of reflector thickness influences the reflection window of the frequency,[9] but the simulation in the present work shows that for the

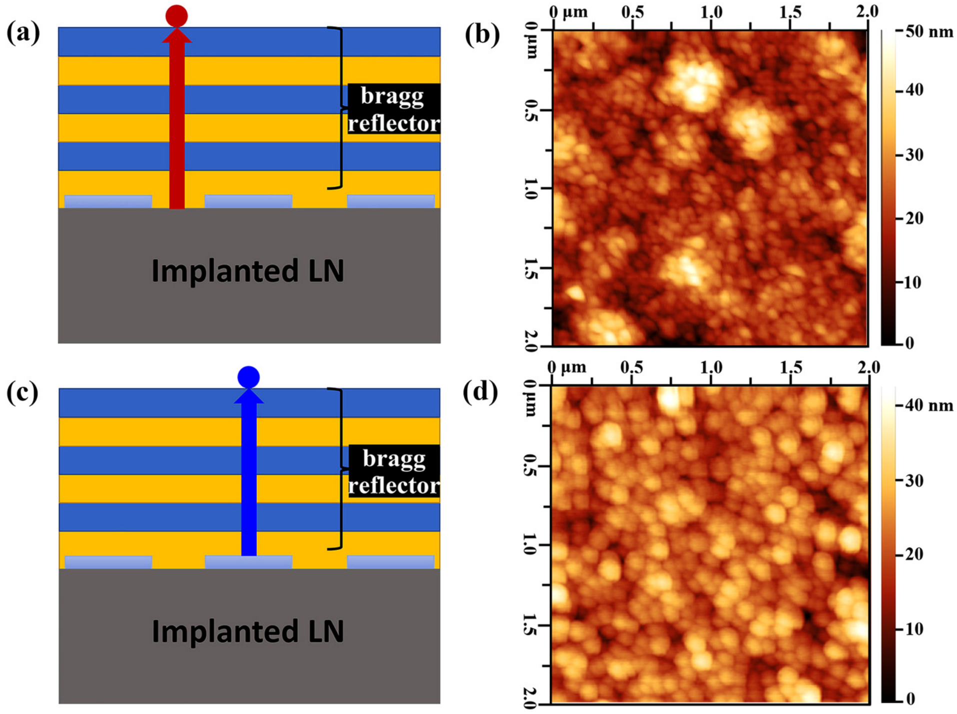

FIG. 2. (a) The region above the bare implanted LN, (b) the surface morphology of region (a), (c) the region above the Al bottom electrode, and (d) the surface morphology of region (c).

resonator working at 3.3 GHz, this thickness deviation does not have a significant influence.

Al top electrodes are finally sputtered onto the LN thin film with a G-S-G geometry, and the resulted BAW resonator is illustrated in Fig. 4(a), the structure parameters of the device are summarized in Table I. The S11 parameter of the device is measured by a network analyzer, and the return loss is −3 dB [Fig. 4(b)]. The deduced input impedance curve is shown in Fig. 4(c), it can be seen that the resonant frequency (f_s) and anti-resonant frequency (f_p) are 3.099 GHz and 3.323 GHz, respectively, which are much higher than the devices based on mechanically polished LN layer reported before.[8] The impedance ratio defined as Z_p/Z_s is more than 50 dB, which is much higher than other reported BAW resonators with the Bragg reflector.[10–12] In addition, no spurious resonance state is observed in a frequency range of 2.5–4.5 GHz, indicating that the 43° rotated Y-cut LN thin film has a pure longitudinal resonance.

To evaluate the effect of the Mo/Ti reflector, it is important to calculate the Q factor of the device. As shown in Fig. 4(d), the Q factors at f_s and f_p are calculated to be ∼183 and ∼168, respectively. More importantly, the K_t^2 of the LN film, calculated by the formula $K_t^2 = \frac{\pi^2}{4}\frac{f_p - f_s}{f_p}$, is ∼16.63%, which is much higher than AlN (∼6.5%), demonstrating that the 43° rotated Y-cut LN thin film is promising for wideband applications. Note that the figure-of-merit ($FOM = Q^*K_t^2$) is also used to evaluate the resonator property,[13] and the FOM of our resonator reaches 30.4 [FOM(f_s)] and 27.9

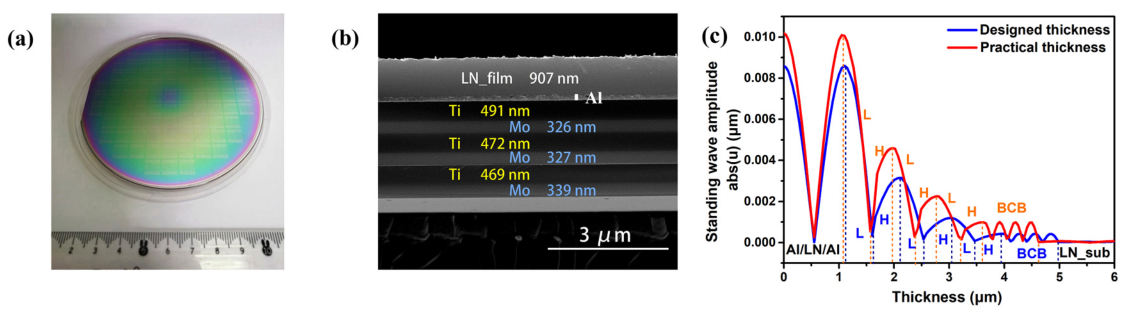

FIG. 3. (a) A 4-in. LN thin film with the bottom Al electrode and the Mo/Ti Bragg reflector, (b) cross-sectional image of the LN thin film and the metallic multilayers, and (c) the distribution of standing wave amplitude based on designed thicknesses (blue curve) and practical thicknesses (red curve).

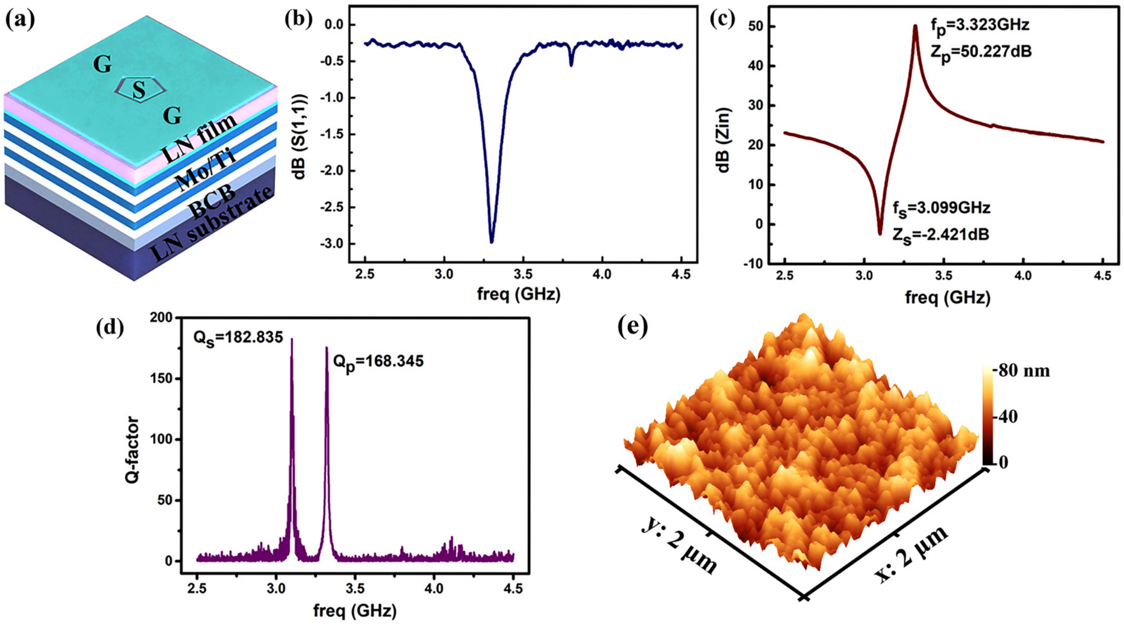

FIG. 4. (a) Configuration of the LN-BAW resonator with the Mo/Ti Bragg reflector, (b) measured S11 curve of the resonator, (c) input impedance curve of the resonator, (d) Q-factor of the resonator, and (e) surface morphology of the LN thin film tested by AFM.

[FOM(f_p)], which are comparable or higher than some reported resonator based on the AlN, BST, or ZnO piezoelectric layer.[14–17] In addition, note that the K_t^2 calculated by the tested result is lower than the theoretical value,[4] that is likely due to two reasons: first, the transferred LN thin film experienced high energy implantation, although the implanted ion (He^+) does not have a high quantity, lattice damage of the LN crystal is inevitably introduced, which deteriorate the piezoelectric performance of the LN thin film. Second, the LN thin film is exfoliated from a LN wafer, and there is a thin amorphous layer on the surface of LN films caused by the intensively accumulated layer of implanted ions. Thus, the split surface has a large roughness, which was reported in previous work.[18] As shown in Fig. 4(e), the RMS of the LN thin film is ∼11.5 nm. This rough surface may cause a spread reflection of the acoustic wave, which lowers the conversion efficiency from electrical energy to longitudinal acoustic energy. The possible solutions are post-annealing and chemical mechanical polishing (CMP) of the LN thin film after transferring, the former reconstructs the damaged LN lattice to some extent, and the latter removes the amorphous layer and flattens the splitted surface of the LN thin film.[19] Thus, both post-annealing and CMP are beneficial to further raise the K_t^2 of the transferred LN thin film.

TABLE I. Structure parameters of the BAW device.

Material	Thickness (μm)
Top Al	0.1
LN thin film	0.9
Bottom Al	0.2
Ti (three layers)	0.46
Mo (three layers)	0.47
BCB	1
LN substrate	500

IV. CONCLUSION

LN-BAW devices based on the Mo/Ti Bragg reflector and the 43° rotated Y-cut LN thin film are fabricated successfully by means of CIS technique and BCB bonding method. The transferred LN film coated with Mo/Ti multilayers is crack-free, and there is a good acoustic reflection efficiency for the Mo/Ti Bragg reflector. Moreover, Mo/Ti-based LN-BAW provides a large K_t^2 of ∼16.63%, and the Q-factor and FOM reach 183 and 30.4, respectively. However, the K_t^2 may have been reduced by lattice damage and damage layer introduced by the process of ion implantation. Therefore, it is necessary to further optimize the process by introducing post-annealing and CMP on the LN film.

ACKNOWLEDGMENTS

This work was supported by the National Key Research and Development Plan (No. 2017YFB0406402) and the National Natural Science Foundation of China (No. 51772044).

DATA AVAILABILITY

The data that support the findings of this study are available from the corresponding author upon reasonable request.

REFERENCES

[1]F. Z. Bi and B. P. Barber, IEEE Microw. Mag. **9**(5), 65–80 (2008).
[2]C. Yang, K. Uehara, S. Kim, and S. Kameda, H. Nakase, and K. Tsubouchi, paper presented at the IEEE Symposium on Ultrasonics (2003), pp. 170–173.
[3]M. A. Moreira, J. Bjurström, V. Yantchev, and I. Katardjiev, IOP Conf. Ser. Mater. Sci. Eng. **41**, 012014 (2012).
[4]T. Baron, E. Lebrasseur, F. Bassignot, H. Wang, S. Ballandras, J. Fan, L. Catherinot, M. Chatras, P. Monfraix, and L. Estagerie, Int. J. Microw. Sci. Technol. **2013**, 1–6 (2013).
[5]A. Guarino, G. Poberaj, D. Rezzonico, R. Degl'Innocenti, and P. Gunter, Nat. Photonics **1**(7), 407–410 (2007).
[6]G. Poberaj, M. Koechlin, F. Sulser, A. Guarino, J. Hajfler, and P. Günter, Opt. Mater. **31**(7), 1054–1058 (2009).
[7]Y. Shuai, C. Gong, X. Bai, C. Wu, W. Luo, R. Böttger, S. Zhou, B. Tian, and W. Zhang, Jpn. J. Appl. Phys. **57**(4S), 04FK05 (2018).
[8]M. Pijolat, S. Loubriat, S. Queste, D. Mercier, A. Reinhardt, E. Defaÿ, C. Deguet, L. Clavelier, H. Moriceau, M. Aïd, and S. Ballandras, Appl. Phys. Lett. **95**(18), 182106 (2009).
[9]S. Jose, A. B. M. Jansman, and R. J. E. Hueting, paper presented at the 2009 IEEE International Ultrasonics Symposium (2009), pp. 2111–2114.
[10]T. Mirea, J. Olivares, M. Clement, J. Sangrador, and E. Iborra, paper presented at the 2018 IEEE International Ultrasonics Symposium (IUS) (2018), pp. 1–4.
[11]A. Roy, B. P. Barber, and K. Prasad, paper presented at the 2010 23rd International Conference on VLSI Design (2010), pp. 170–175.
[12]H. Xu, Y. Su, H. Yang, D. Xu, Y. Zhang, D. Chen, and Y. Liu, paper presented at the 2012 Fourth International Symposium on Information Science and Engineering (2012), pp. 183–186.
[13]R. Ruby, "Review and comparison of bulk acoustic wave FBAR, SMR Technology," *Ultrasonics Symposium Proceedings* (IEEE, 2007), pp. 1029–1040.
[14]T. Mirea, J. Olivares, M. Clement, J. L. Olivera, J. Sangrador, and E. Iborra, in *2017 Joint Conference of the European Frequency and Time Forum and IEEE International Frequency Control Symposium (EFTF/IFCS)* (IEEE, 2017), pp. 519–522.
[15]T. S. Kalkur, M. Hmeda, A. Mansour, P. Alpay, N. Sbockey, and G. S. Tompa, paper presented at the 2015 Joint Conference of the IEEE International Frequency Control Symposium & the European Frequency and Time Forum (2015), pp. 392–395.
[16]Y. Liu, Y. Shen, F. Duan, Y. Zhang, Z. Li, H.-L. Hwang, and Y. Zhang, Vacuum **141**, 254–258 (2017).
[17]H. M. Edrees, A. R. Colón-Berrios, D. G. Peixoto, K. L. Shepard, P. R. Kinget, and I. Kymissis, J. Microelectromech. Syst. **26**(4), 846–858 (2017).
[18]X. Y. Bai, Y. Shuai, C. G. Gong, C. G. Wu, W. B. Luo, R. Bottger, S. Q. Zhou, and W. L. Zhang, Appl. Surf. Sci. **434**, 669–673 (2018).
[19]B. Imbert, A. Reinhardt, T. Ricart, C. Billard, M. Pijolat, E. Defaÿ, E. Augendre, T. Signamarcheix, and C. Deguet, paper presented at the 2011 Joint Conference of the IEEE International Frequency Control and the European Frequency and Time Forum (FCS) Proceedings (2011), pp. 1–4.